Indian Journal of Pure & Applied Physics
Vol. 62, March 2024, pp. 212-221
DOI: 10.56042/ijpap.v62i3.6789

Effect of Post Air Annealing on the Characteristics of Spray Deposited ZnO Thin Films and Their use as MOS Ethanol Gas Sensor

Prakasha G S[a*], Shashidhar R[b] & Madhukeswara R S[c]

[a]Department of Physics, Global Academy of Technology (Affiliated to Visvesvaraya Technological University), Bangalore 560 098, India

[b]Department of Physics, J S S Academy of Technical Education (Affiliated to Visvesvaraya Technological University), Bangalore 560 060, India

[c]Department of Physics, Government College for Women (Autonomous) (Affiliated to Mandya University), Mandya 571 401, India

Received 18 November 2023; accepted 19 January 2024

Spray Pyrolysis (SP), a low-cost chemical procedure was employed to deposit ZnO thin films under optimum conditions at 350 °C using a predetermined precursor concentration of 0.1 M. This study investigates how post-air annealing affects the structural, compositional, morphological, optical, and electrical properties of ZnO thin films. The deposited films were heated by air at 400, 450 and 500 °C for 1 h. X-ray diffraction, scanning electron microscope, x-ray dispersive spectroscopy, Raman spectroscopy, Fourier Transform Infrared Spectroscopy, optical spectroscopy, and Hall effect studies were conducted to investigate how post-air annealing alters the properties of the as-deposited film. XRD measurements show that annealing resulted in the growth of polycrystalline hexagonal wurtzite without the formation of any other phases in ZnO films. When heated to 500 °C, the estimated crystallite size of the as-deposited film increased from 6.22 nm to 6.57 nm. The SEM show the creation of compact and tightly packed films, as well as the visible network of large grains during annealing. Raman and FTIR studies have validated the chemical structure, molecular interactions, and formation of chemical bonds in ZnO thin films. Optical studies show that the energy band gap widens during annealing. Optical profilometer studies verified the uniformity of the deposited film surface. According to Hall effect analysis, conversion of p to n type occurs at an annealing temperature of 450 °C. A ZnO-based MOS gas sensor was found to have better selectivity towards C_2H_5OH than other test gases such as NH_3, NO_2, and H_2S. At room temperature, the sensor response and recovery time is shorter for NH_3 than for C_2H_5OH test gas. In environmental monitoring, the present gas sensor can detect ethanol.

Keywords: ZnO; Spray pyrolysis; Annealing; P type; Gas sensor

1 Introduction

ZnO nanofilms are currently used in lighting, electronics, photonics, and photocatalysis. Its strong chemical stability, broad bandgap of 3.37 eV, high exciton binding energy of 60 MeV, adequate occurrence in nature, and safety are among its advantages that are well acknowledged[1,2]. Physical and chemical synthesis are the two primary methods for producing high-quality ZnO films. Sputtering[3], molecular beam epitaxy[4], and laser ablation[5] are examples of physical techniques. Spray pyrolysis[6,7], sol-gel[9], chemical vapour deposition[8], spin coating[10], dip coating[11], and electrodeposition[12] are a few examples of chemical methods. Most of the strategies discussed in the literature are not ideal for covering large areas. But according to earlier research[3-12], Spray Pyrolysis (SP) is one of the most effective process for producing large-area coatings. Additionally, it possesses high levels of purity, low deposition temperatures, economical, and great film-to-substrate adhesion[13]. Some of the key variables influencing the properties of the spray pyrolysis-coated film include the chemical solution (chemical composition, concentration), the separation between the substrate and the atomizer, interaction during film deposition, spray temperature, substrate homogeneity, annealing conditions, and spray rates[14]. SP is an effective, low-cost process for depositing thin films, multilayer films, thick films, and porous films on a substrate[13]. This process has been used to deposit several oxides, including ZnO[15], CdO[16], TiO_2[17], SnO_2[18], NiO[19], and Bi_2O_3[20]. A heated substrate is sprayed with a water or alcohol solution containing metal salts, which is then allowed to cool until an oxide layer forms. Oxide is a thermodynamically viable outcome of the breakdown reaction, leaving no traces of the remaining reactants. The temperature of the substrate has a significant impact on the film form. As the temperature rises, the film morphology may change from fragmented to porous[21]. The kinds

*Corresponding author: (E-mail: gsprakasha@gat.ac.in)

and amounts of additive and precursor components have a big impact on how things are organised and what they do[22]. The unannealed spray-deposited film has poor transparency, low roughness, and high resistance because of the organic residues and low crystallinity it contains[23-25]. Thermal annealing, plasma therapy, and laser treatment can improve the properties of an unannealed film[26-27]. Out of these options, the thermal annealing procedure is one of the simplest and most effective ways to manage the spray-deposited films. The thermal annealing temperature, time, and various gaseous environments influence film and the structural faults in the material.

Since thermal annealing retains dislocations and other structural faults, besides any adsorption or surface breakdown, it changes the material's structure and stoichiometric ratio[28]. The following faults are typically present in coated ZnO films: excess oxygen, excess zinc, oxygen, and zinc interstitial. The faults that occur more frequently[29,30] are zinc interstitial and oxygen vacancies. In the Nunes and group study, using zinc acetate as a precursor[31,32], investigations on the structural, optical, and electrical properties of doped and undoped ZnO thin films in various contexts were made. According to Yoon and Chou[33], zinc acetate dehydrate was used as a precursor to prepare ZnO thin films and studies were done about how different substrate temperatures and heat treatments affected the luminous properties of the ZnO layer and discussed their findings. Ayouchi *et al*[34]. have discussed the influence of substrate temperature on the physical features of ZnO thin film,

Metal oxide nanostructure-based gas sensors have been extensively researched and used in a wide range of applications ranging from health and safety to emission control[35-39]. These sensors are appealing because of their excellent sensitivity, cost effectiveness, simplicity, and compatibility with recent electronic devices due to direct electrical readouts[40]. Until now, several metal oxides such as TiO_2, In_2O_3, WO_3, ZnO, TeO_2, CuO, SnO_2, and NiO have been utilized in resistive-type metal oxide gas sensors[41]. These single metal oxide gas sensors, on the other hand, typically have low sensitivity, a high operating temperature, and poor gas selectivity[42]. There is pressing need to develop highly sensitive methods for detecting toxic and hazardous gases. Because of its superior physicochemical properties, ZnO is widely used as a gas sensing material for detecting toxic and harmful gases[43].

Although a few factors might have an impact on the film structure, we are unsure of how the annealing temperature affects the ZnO films coated by SP. This work investigates how undoped ZnO film structural, morphological, compositional, optical, and electrical characteristics are affected by air annealing and as well as the use of as-deposited ZnO film on ITO as a simple MOS gas sensor.

2 Experimental details

2.1 Preparation of ZnO Thin films

The cleanliness of the substrate affects any device's performance, as a result, the substrates were cleaned in the manner detailed below. With DI water, acetone, and chromic acid, glass and quartz substrates of 1 cm^2 area are pre-cleaned. Si substrates of equal size were pre-cleaned using the RCA1 and RCA2 techniques. ITO substrates of dimension 1.5 cm × 1 cm were cleaned with DI water and NaOH solutions, respectively.

To deposit ZnO thin films, the precursor solution of ZnO is prepared as follows: To prepare a 0.1M ZnO solution, 2.195g of zinc acetate dihydrate [Zn $(CH_3COO)_2 2H_2O$]. Loba Chemicals Pvt. Ltd. is dissolved in 30 ml of double-distilled water and 90 ml of isopropyl alcohol (99% assay). At room temperature, the mixture is stirred for ten minutes.

Figure 1 displays the schematic representation of the SPD setup. ZnO thin films were coated utilising a homemade Spray Pyrolysis Deposition (SPD) apparatus under the following optimal conditions: The air pressure and the substrate temperature are set at 4.2 $kgcm^{-2}$ and 350 °C, and the spray nozzle is kept 30 cm away from the substrate. The ZnO precursor solution is sprayed over substrates that have already been cleaned. The deposition is carried out in 36 cycles, with each cycle of duration 5 seconds to maintain the deposition temperature at 350 °C. To find out more about how annealing affects the properties of the coated thin films, films are air annealed at 400, 450 and 500 °C for 1 hour.

In order to study and figure out the ZnO properties, thin films are coated on various types of substrates. Coated glass plates, quartz plates, and Si substrates are utilised for electrical, optical, XRD, Raman, FTIR, SEM, and EDS characterizations. ITO coated Glass plates are employed in gas sensing studies.

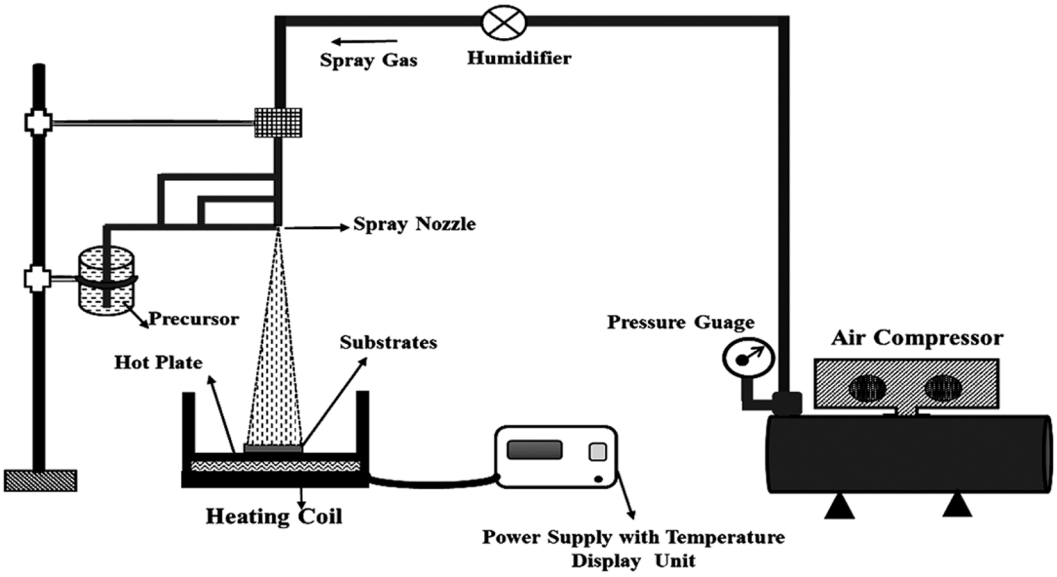

Fig. 1 — Schematic diagram of Homemade SPD setup.

3 Results and Discussion

3.1 XRD analysis

In their research, Seeley *et al*., found that higher crystallinity increases the ability to detect gas/chemical species. Hence XRD analysis is done on both as deposited and air annealed thin films. This is also done to see how heating changes the crystallinity of ZnO thin films. The XRD diffraction patterns of ZnO thin films coated by spray pyrolysis and air annealed for an hour at varied temperatures of 400, 450, and 500 °C are depicted in Fig. 2. Prominent XRD peaks were observed at 2θ (hkl) = 31. 89°(100), 34.48°(002), 36.4°(101), 47.58°(102), 56.4°(110) and 63.02°(103). The polycrystalline hexagonal wurtzite structure of the ZnO thin film is categorically shown by this finding[45] (as per JCPDS card No. 00-036-1451). ZnO thin film polycrystalline nature is suggested by a strong (002) preferred orientation. These findings were noted by[45] Raied *et al*., (2014). Notably, the peak intensity during air annealing reaches its highest at a temperature of 450 °C before beginning to decline. At the 2θ values mentioned above, it was observed that the crystallinity index improved. The crystallite size was found to grow with air annealing[46] because of FWHM variation. It was shown that the peak intensities of the XRD at 2θ = 34.48° and 36.4° at 450 °C were nearly equal.

Many researchers have reported that structural properties such as dislocation densities, grain size, micro strain, and crystallinity index influence gas sensing in metal oxide semiconductors[47-50]. As a result, it is decided to conduct structural studies.

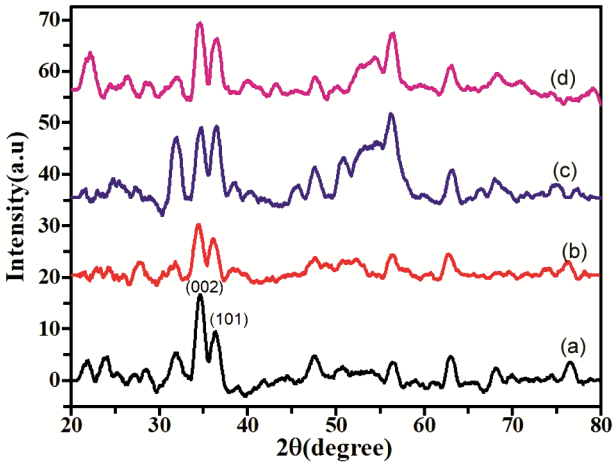

Fig. 2 — XRD patterns of the Spray deposited air annealed ZnO thin films.

Table 1 displays the structural parameters of spray-deposited, air-annealed ZnO thin films. The crystallinity index was seen to rise during annealing. In addition to grain boundaries, grain size variation may be the cause of the significant dislocation density and microstrain seen at 450 °C. The dislocation density and microstrain are found to be at their maximum values at 450 °C, while the crystallite size and interplanar spacing are found to be at their lowest values at 2θ =34.48°. Air annealing has resulted in an increase in crystallite size[51,52]. Changes in dislocation density and microstrain may be attributed to crystallisation and crystal defects[53].

Table 1 — Structural parameters of the Spray deposited air annealed ZnO thin films.

Crystal size, $D = \frac{k\lambda}{\beta\cos\theta}$, nm	Interplanar spacing, $d = \frac{\lambda}{2\sin\theta}$, nm	Dislocation density, $\delta = \frac{1}{D^2}$, nm^{-2}	Crystallinity Index(CI)	Micro Strain, $\varepsilon = \frac{\beta}{4\tan\theta}$
6.227	0.259	0.026	0.518	0.0187
6.183	0.259	0.026	0.480	0.0188
5.803	0.258	0.030	0.559	0.0200
6.570	0.259	0.023	0.676	0.0178

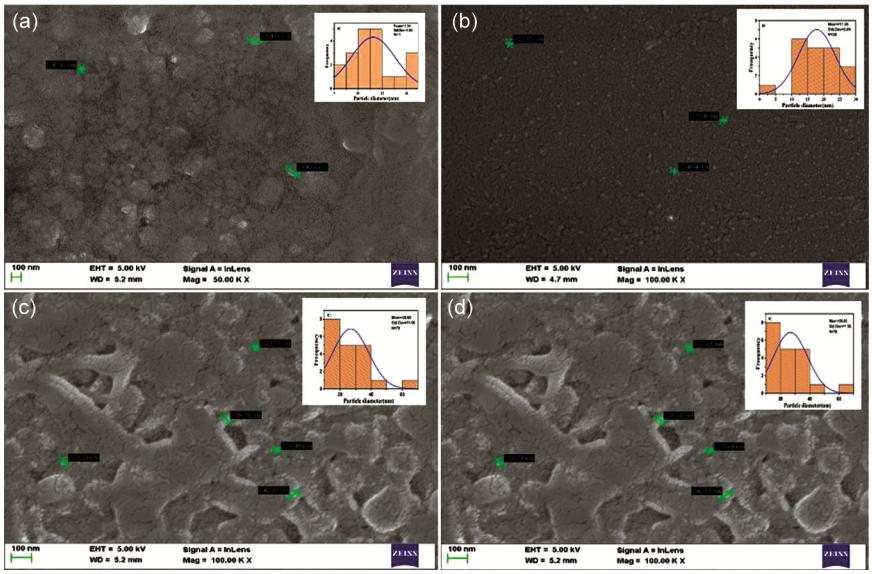

Fig. 3 — Scanning Electron Micrographs of spray deposited air annealed ZnO thin films.

3.2 SEM & EDS analysis

SEM studies were performed to analyse the micrograph because smaller grain sizes have superior sensing properties[54]. Fig. 3 depicts the SEM images of as deposited and air annealed ZnO thin films. As deposited films appear compact and densely packed. Air annealing up to 400 °C appears to increase grain size with time. Continued annealing causes grain size to increase above 400 °C, but surprisingly, channels or networking of grains, some flakes, and voids were also observed in the films.

Formation of interconnected 3D network with electronic connections may help charge transportation. As the annealing temperature rises, more activated dislocations will form, gradually reducing the density of dislocations. The grain size also becomes larger[52]. Stoichiometry in films is critical because it affects electronic structure, material properties, and especially electrical transport, all of which can affect sensor gas sensing behaviour[55]. By using EDS stoichiometric analysis, Zn and O elements are confirmed, and no other impurity elements were found in the as deposited films[56].

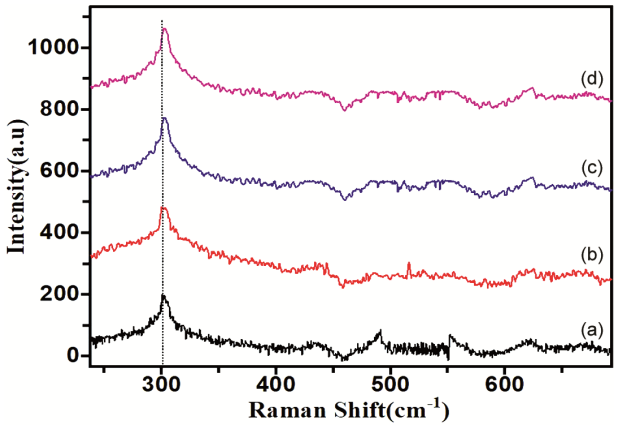

Fig. 4 — The Raman spectra of as-deposited and air annealed spray deposited ZnO thin film.

3.3 Raman analysis

The Raman spectra are like "fingerprints" for molecules, and they are very useful for identifying chemical structure and detecting vibrational modes of molecules that are not IR active. Fig. 4 displays the Raman scattering spectra of spray deposited, air annealed ZnO thin films stimulated by 2 mW laser lines at 532 nm. A significant peak of 301.44 cm^{-1} has

been observed in the as deposited ZnO film[57]. A 301.44 to 302.35 cm^{-1}. Raman shift was observed as the as deposited film was air annealed; this could be associated to the growth of nanocrystals inside the ZnO thin films. Along with this strong peak, smaller peaks were also observed at 432.25, 492.73, 552.72, 624.86 and 669.70 cm^{-1}. It has been established that air annealing increases peak intensity. The Raman peak intensity may be improved as the annealing temperature is increased owing to the development in the crystallinity of films. The surge in surface roughness is an indication to the rise in grain size on subsequent annealing of the films. The unique ZnO nanoparticle peaks at 220, 323, 437 and 620 cm^{-1} were visible in the Raman spectra. While the E_2 mode causes the peak at 437 cm^{-1}, the peak at around 332 cm^{-1} is caused by the second-order structure of zinc oxide (ZnO)[58].

The hexagonal ZnO E_2 (high) mode is linked to this peak. When ZnO film is annealed in the air for one hour at 500 °C, two peaks are seen. The E_2 (low) mode and E_2 (high) modes made of hexagonal ZnO are indicated by the Raman peaks at 100 cm^{-1} and 436.5 cm^{-1}, respectively[59,60]. After annealing, the FWHM of the E_2 peak decreased. In wurtzite ZnO crystals, the non-polar phonon modes with symmetry E_2 have two frequencies: E_2, which is tied to the Zn sublattice and E_2 (low), which is connected to oxygen atoms[61-64,65].

3.4 FTIR analysis

FTIR is a powerful analytical tool for detecting functional groups and characterising covalent bonding information on the surface of a film. The FTIR data is useful for analysing the interaction of gas molecules at the film's surface. The FTIR spectra of as-deposited and air-annealed ZnO thin films are shown in Fig. 5. Transmission was seen at 2917, 2316, 1590, 1135, 1067, and 607 cm^{-1}. As per the graph, the transmission is at its highest values at 450 °C. At 400 °C and 450 °C, transmission is observed at 1590 and 2316 cm^{-1}, which is attributable to air annealing. At 1130 cm^{-1}, the transmission found to decrease with annealing[66]. The transmission around 3000, 1600-1500, 900 and 600 cm^{-1}[67,68,69], may be ascribed to –OH stretching, C-H vibrations, C=O vibrations, -OH stretching, and Zn-O bonding respectively.

3.5 Optical analysis

The optical studies provide the porosity in films, which determines the sensitivity of the gas sensor. Table 2 displays the optical analyses of spray-deposited, air annealed, undoped ZnO thin films. Measurements of optical parameters are conducted at λ= 600 nm. Annealing was found to increase the optical band gap and porosity. The absorption coefficient, optical conductivity, and imaginary component of the dielectric constant, on the other hand, all appeared to be high at 450 °C. The temperature related change in grain size is the cause for the fluctuation in optical properties. The optical bandgap found to vary from 3.21-3.59 eV[70]. Films with increased porosity provide superior gas sensing. Another benefit of prepared films is higher

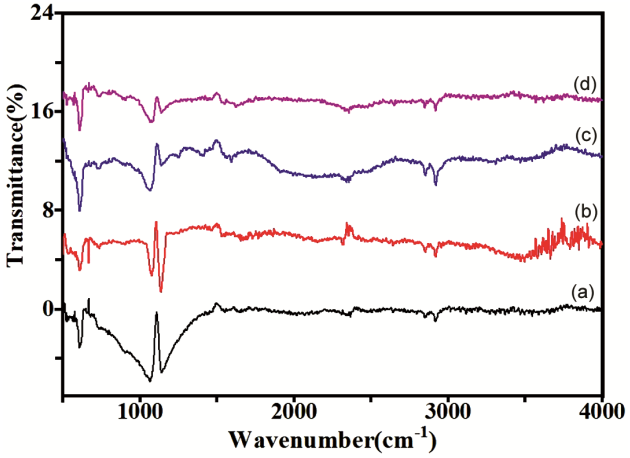

Fig. 5 — FTIR spectra of as deposited and air annealed spray deposited ZnO thin film.

Table 2 — Optical parameters of the Spray deposited air annealed ZnO thin films

T, ^{0}C	Film thickness (t) nm	$\alpha = \frac{2.302 \times T}{t}$ $10^5, m^{-1}$	E_g, eV	Porosity % $\phi = \left[1 - \frac{n_f^2 - 1}{n_b^2 - 1}\right] \times 100$	Extinction coefficient t $k = \frac{\alpha\lambda}{4\pi}$	Optical susceptibility $\chi = \frac{n^2 - k^2 - 1}{4\pi}$	Optical conductivity $\sigma = \frac{\alpha nc}{4\pi}$ 10^{12}	Packing density P= $\frac{(n_f^2-1)(n_b^2+2)}{(n_f^2+2)(n_b^2-1)}$	Real Part of Dielectric Constant $\varepsilon_r = 1 + 4\pi\chi$	Imaginary Part of Dielectric Constant $\varepsilon_i = 2nk$
350	363.79	1.36	3.21	91.91	0.007	0.124	5.2	0.4910	2.5530	0.0208
400	360.38	3.09	3.38	93.49	0.015	0.115	11.52	0.4680	2.4453	0.0461
450	324.12	3.43	3.45	93.49	0.016	0.115	12.8	0.4680	2.4453	0.0512
500	367.62	0.24	3.59	93.45	0.001	0.115	0.912	0.4683	2.4477	0.0036

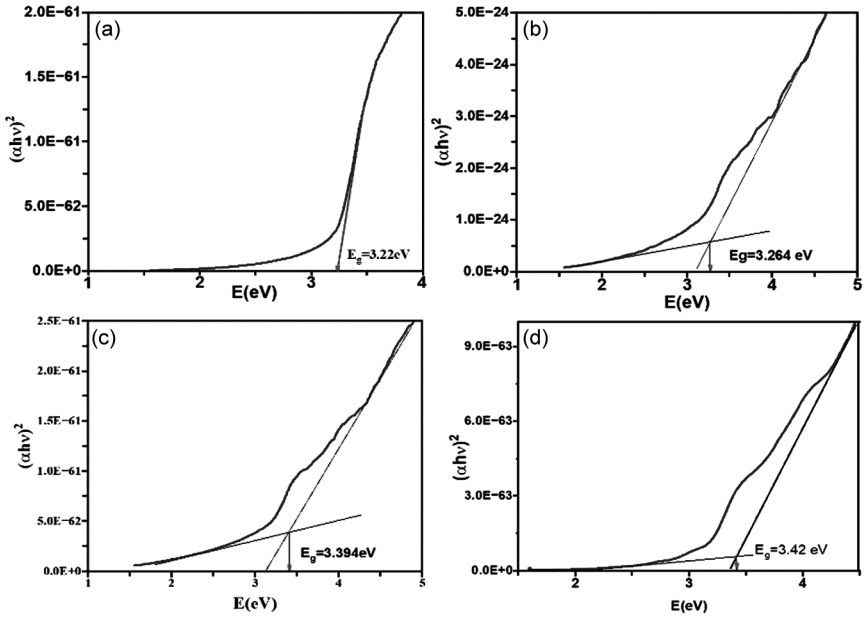

Fig. 6 — UV-Vis spectra of as deposited and air annealed spray deposited ZnO thin film.

Table 3 — The electrical properties of spray as deposited, and air annealed undoped ZnO thin films

T, ^{0}C	Grain size, nm	R_s $10^9\Omega$	Thickness, t, nm	Resistivity $\rho = R_S t$, $10^3\,\Omega$ m	V_H, V	$R_H = \frac{V_H W}{BI}$ 10^3 m^{3}C^{-1}	$n_s = \frac{1}{R_H e}$ 10^{15}m^{-2}	$n = n_S/t$ 10^{22}m^{-3}	$p = p_S/t$ 10^{22}m^{-3}	Mobility, $\mu = \frac{1}{R_S n_s e}$ 10^{-7}m^2/V-s	Material Type
350	11.24	6.67	363.79	2.43	1.46	1.46	4.27		1.175	2.19	p
400	17.85	0.95	360.38	0.34	0.76	0.76	8.26		2.295	7.99	p
450	26.83	4.49	324.12	1.45	-4.014	-4.01	-1.56	-0.481		-8.93	n
500	23.82	0.89	367.62	0.33	-4.005	-0.57	-10.92	-2.971		-6.39	n

transmission, which is necessary for a window in a solar cell. The optical studies show that the synthesised films can be used to fabricate both gas sensors and solar cells. Fig. 6 shows the UV-Vis spectra of the different samples.

3.6 Electrical analysis

The electrical analyses of spray deposited, air annealed, undoped ZnO thin films are shown in Table 3. As per the positive hall voltage at 350 and 400 °C obtained films have p type conductivity and poor hole mobility. However, at 450 and 500 °C, the resultant films do shows n-type conductivity and have weak electron mobility. It was found that the bulk and sheet charge concentrations were about 10^{22}m^{-3} and 10^{15}m^{-2}, respectively. One-order variation in sheet resistance and charge concentration is observed because of improvement in grain size with air annealing. The dense structure and the removal of defects with oxygen insertion may also contribute to the significant sheet resistance[65]. The electrical study clearly shows that the ZnO film conductivity can be easily converted from p to n type with meagre post air annealing without employing expensive dopants such as CO[66-71]. The identification of material type by hall effect is critical, as Wisitsoraat *et. al.* reported that p type semiconductor-based gas sensor found to be better than n -type[72]. The Table 3 also includes information about sheet resistance and mobility, which clearly explains charge transportation at the interface during gas molecule sensing.

3.6 Sensing analysis

3.6.1 Fabrication of MOS sensor

ZnO thin films deposited on the conducting side of an ITO coated glass plate used as a MOS gas sensor. Fig. 7 depicts the schematic diagram of the fabricated MOS sensor The silver paste dot is applied one on the surface of ZnO thin films and the other in the masked area of the ITO glass plate. Two copper wires were taken from the silver paste for electrical connections during the gas sensing studies. Fig. 8 depicts a

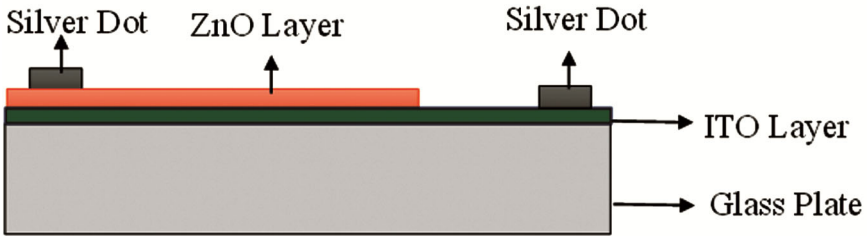

Fig. 7 — Schematic diagram of fabricated ZnO based MOS sensor.

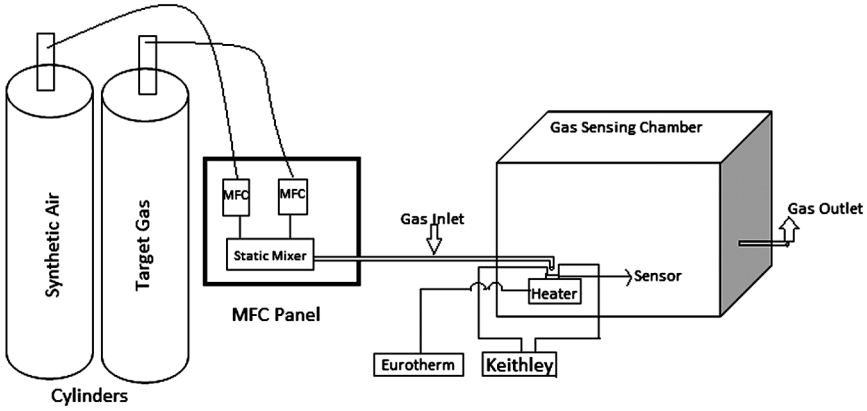

Fig. 8 — Schematic diagram of Gas sensing calibration setup.

schematic diagram of the gas sensing calibration setup used in this study.

3.6.2 Selectivity studies of ZnO based MOS sensor

5 ppm of various test gases such as ammonia (NH_3), ethanol (C_2H_5OH), nitrogen dioxide (NO_2), and hydrogen sulphide (H_2S) were employed to analyze the gas sensing behaviour of the fabricated sensor at room temperature. The selectivity studies on the ZnO thin film MOS gas sensor was performed at Room Temperature (RT) by purging 5ppm of the above test gases, and the plot is as presented in Fig. 9. Current through the MOS sensor is measured by passing synthetic gas (I_a) and test gas (I_g) during a downward trend. The sensitivity (S %) is measured employing the measured values of current, using the Eq., $S(\%) = \frac{(I_a - I_g)}{I_g} \times 100$. The measured current was found to be stable throughout the study. The sensitivity measured (Table 4) for ethanol is 2%, compared to 1% for other gases. Nag *et al*., reported in their work that the sensitivity of gas enhances if the crystal size is less than 5 nm, but XRD shows it to be around 6 nm[73]. Out of 4 test gases, the sensor was observed to exhibit low but better selectivity for ethanol. The sensing study shows that ethanol proved to be a selective gas for the fabricated sensor.

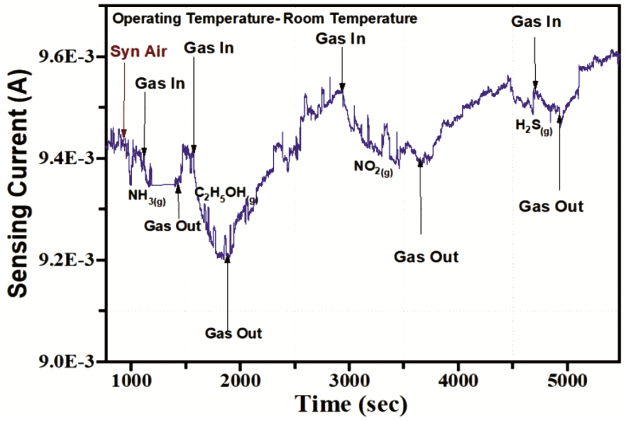

Fig. 9 — Selectivity studies on fabricated ZnO based MOS sensor at room temperature.

Table 4 — Selectivity studies on ZnO based MOS gas sensor

Gas	I_a, mA	I_g, mA	S	S%	Observation
NH_3	9.40	9.35	0.01	1	-
C_2H_5OH	9.40	9.20	0.02	2	Selective gas
NO_2	9.54	9.48	0.01	1	-
H_2S	9.53	9.39	0.01	1	-

Sensing mechanism: When ethanol is purged, the surface oxygen species reacts with the ethanol molecules, releasing the chemisorbed electrons to the films. Consequently, the net resistance of the film decreased rapidly[74]. Changes in band gap, work

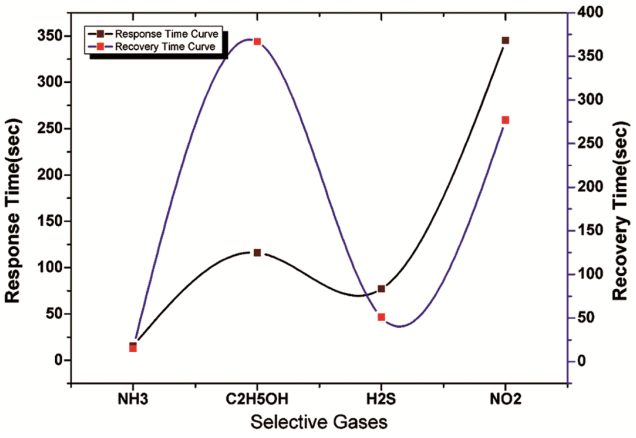

Fig. 10 — Response and Recovery time as a function of test gases.

function, and electron affinity of ZnO thin films can be ascribed to Fermi electron transfer across the film surface and gas molecules[75]. As a result, sensor sensitivity to ethanol is increased.

Cost effective room temperature MOS sensor fabricated using SPD found to be reasonably sensitive at 5ppm of ethanol, and far better than that prepared by expensive hydrothermal process which is sensitive to 50 ppm at higher operating temperature[76]. Even after several trials, the current through the MOS sensor was found to be stable. The current ethanol sensor can be used in environmental monitoring to detect ethanol. Gas sensing research on air annealed ZnO thin film-based MOS gas sensors is currently underway.

The response and recovery time of a fabricated gas sensor as a function of test gases are shown in Fig. 10. For ethanol, the sensor's response and recovery time are 116 and 367 seconds, respectively, whereas for ammonia, it is 15.5 and 15 seconds. Even though the sensor is more sensitive to ethanol, when ammonia gas is purged into the gas chamber, the speed is high. Because of their huge amount of surface sites that facilitate surface reactions, nanomaterials such as nanorods, nanowires, nanoflakes, nanoflowers, and nanoparticles have dominated research interest in gas sensing applications. Hence, the sensitivity of a gas sensor may vary depending on the surface reaction[77]. The ethanol sensor speed can be increased further by modifying the ZnO nanostructure and varying the operating temperature, film thickness, doping, and metal work function.

4 Conclusion

Spray pyrolysis was effectively employed to deposit ZnO thin films, which were then thermally post air annealed in a muffle furnace at varied temperatures. The XRD, SEM, EDS, Raman, FTIR, UV-VIS-IR spectrophotometer and Hall effect analysis were used to investigate the structural, morphological, optical, and electrical properties of the ZnO thin films. The film grain size was observed to increase as the annealing temperature increased. As per the XRD diffractogram, the thermally annealed film at 450 °C has an excellent crystalline hexagonal wurtzite structure with a preferential plane orientation along (002). The expected grain size from the SEM examination and the XRD data are frequently in agreement. As the annealing temperature is raised, the transmission of the ZnO films increases. ZnO films annealed at 450 °C found to possess strong light transmission of 90% in the visible region. These characteristics of the ZnO film make it advantageous for usage of optoelectronic devices. As per the optical studies, the deposited films can be utilised to fabricate gas sensors and solar cells. Electrical investigations show how films with little charge mobility transferred from p to n type conductivity at an annealing temperature of 450 °C and above. Deposited films were discovered to be stable, to have higher sheet resistance, and to be suitable for gas sensing applications. Undoped ZnO thin films function as a better gas sensor for C_2H_5OH than for NH_3, NO_2 and H_2S test gases. Spray pyrolysis proves to be an effective technique for mass-production of low-cost MOS gas sensor. The sensor responds faster to ammonia than to the other test gases. In this paper, we report on the selectivity of an as deposited sensor. The effects of air annealing on speed, stability, and sensitivity are being studied and optimised.

Declaration of competing interests

The authors declare that they have no known competing financial interests or personal relationships that could have appeared to influence the work reported in this paper. The authors declare no conflict of interest.

Acknowledgements

The authors acknowledge INUP, IISc., Bangalore for providing characterization facilities and JSSMVP, Mysore, Principals of JSSATE Bangalore, GAT Bangalore and GCW Mandya for their kind support and encouragement. The authors would also like to thank I-STEM, Centre for Nano Science and Engineering, IISc., Bangalore, for funding the research with a catalytic grant through reverse funding.

References

1 Lee J H, Ko K H & Park B O, *J Cryst Growth*, 247 (2003) 119.
2 Könenkamp R, Boedecker K, Lux-Steiner M C, Poschenrieder M & Zenia F, Levy-Clement C & Wagner S, *Appl Phys Lett*, 77 (2000) 2575.
3 Eisermann S, Sann J, Polity A & Meyer B K, *Thin Solid Films*, 517 (2009) 5805.
4 Look D C, Reynolds D C, Litton W C, Jones R L, Eason D B & Cantwell G, *Appl Phys Lett*, 81 (2002) 830.
5 Hiramatsu M, Imaeda K, Horio N & Nawata M, *J Vac Sci Technol A*, 16 (1998) 669.
6 Ayouchi R, Leinen D, Martın F, Gabas M, Dalchiele E & Ramos-Barrado J R, *Thin Solid Films*, 426 (2003) 68.
7 Cuadra J G, Estrada A C, Oliveira C, Abderrahim L. A, Porcar S, Fraga D & Carda J B, *Ceram Int*, 49 (2023) 32779.
8 Fay S, Kroll U, Bucher C, Vallat-Sauvain E & Shah A, *Sol Energy Mater Sol Cells*, 86 (2005) 385.
9 Bao D, Gu H & Kuang A, *Thin Solid Films*, 312 (1998) 37.
10 Srinivasan G, Gopalakrishnan N, Yu Y S, Kesavamoorthy R & Kumar J, *Superlattices Microstruct*, 43 (2008) 112.
11 Brinker C J, Frye G C, Hurd A J & Ashley C S, *Thin Solid Films*, 201 (1991) 97.
12 Dalchiele E A, Giorgi P, Marotti R E, Martın F, Ramos-Barrado J R, Ayouci R & Leinen D, *Sol Energy Mater Sol Cells*, 70 (2001) 245.
13 Perednis D & Gauckler L J, *J Electroceram*, 14 (2005) 103.
14 Korotcenkov G, Brinzari V, Schwank J & Cerneavschi A, *Mater Sci Eng C*, 19 (2002) 73.
15 Krunks M & Mellikov E, *Thin Solid Films*, 270 (1995) 33.
16 Vigil O, Cruz F, Morales-Acevedo A, Contreras-Puente G, Vaillant L & Santana G, *Mater Chem Phys*, 68 (2001) 249.
17 Natarajan C, Fukunaga N & Nogami G, *Thin Solid Films*, 322 (1998) 6.
18 Brinzari V, Korotcenkov G & Golovanov V, *Thin Solid Films*, 391 (2001) 167.
19 Patil P S & Kadam L D, *Appl Surf Sci*, 199 (2002) 211.
20 Gujar T P, Shinde V R & Lokhande C D, *Mater Res Bull*, 41 (2006) 1558.
21 Chen C, Kelder E M, Van der Put P J J M & Schooonman J, *J Mater Chem*, 6 (1996) 765.
22 Golshahi S, Rozati S M, Martins R & Fortunato E, *Thin Solid Films*, 518 (2009) 1149.
23 Salam S, Islam M, Alam M, Akram A, Ikram M, Mahmood A & Mujahid M, *Nat Sci: Nanosci Nanotechnol*, 2 (2011) 045001.
24 Zhu X, Defaÿ E, Aïd M, Ren Y, Zhang C, Zhu J & Xiao D, *J Phys D Phys*, 46 (2013) 105301.
25 Karamdel J, Dee C F & Majlis B Y, *Sains Malays*, 40 (2011) 209.
26 Yang J, Bei J & Wang S, *Biomater*, 23 (2002) 2607.
27 Du Ahn B, Oh S H, Lee C H, Kim G H, Kim H J & Lee S Y, *J Cryst Growth*, 309 (2007) 128.
28 Wang L, Pu Y, Fang W, Dai J, Zheng C, Mo C & Jiang F, *Thin Solid Films*, 491 (2005) 323.
29 Kang H S, Kang J S, Kim J W & Lee S Y, *J Appl Phys*, 95 (2004) 1246.
30 Sagar P, Shishodia P K, Mehra R M, Okada H, Wakahara A & Yoshida A, *J Lumin*, 126 (2007) 800.
31 Nunes P, Fortunato E & Martins R, *Thin Solid Films*, 383 (2001) 277.
32 Nunes P, Fernandes B, Fortunato E, Vilarinho P & Martins R, *Thin Solid Films*, 337 (1999) 176.
33 Nadarajah K, Chee C Y & Tan C Y, *J Nanomater*, 35 (2000) 39.
34 Ayouchi R, Martin F, Leinen D & Ramos-Barrado, *J Cryst Growth*, 247 (2003) 497.
35 Comini E, Ferroni M, Guidi V, Faglia G, Martinelli G & Sberveglieri G, *Sens Actuators B Chem*, 84 (2002) 26.
36 Lin Y, Wei W, Li Y, Li F, Zhou J, Sun D & Ruan S, *J Alloys Compd*, 651 (2015) 690.
37 Yao M S, Tang W X, Wang G E, Nath B & Xu G, *Adv Mater*, 28 (2016) 5229.
38 Kwak C H, Kim T H, Jeong S Y, Yoon J W, Kim J S & Lee J H, *ACS Appl Mater Interf*, 10 (2018) 18886.
39 Liu D, Pan J, Tang J, Liu W, Bai S & Luo R, *J Phys Chem Sol,* 124 (2019) 36.
40 Miller D R, Akbar S A & Morris P A, *Sens Actuators B*, 204 (2014) 250.
41 Dey A, *Mater Sci Eng B*, 229 (2018) 206.
42 Arafat M M, Haseeb A S M A & Akbar S A, *Comprehens Mater Process*, 13 (2014) 205.
43 Kang Y, Yu F, Zhang L, Wang W, Chen L & Li Y, *Solid State Ion*, 360 (2021) 115544.
44 Seeley Z M, Bandyopadhyay A & Bose S, *Mater Sci Eng B*, 164 (2009) 38.
45 Raied K J, Mohammed A H & Kadhim A A, *Mater Lett*, 132 (2014) 31.
46 Zaier A, Meftah A, Jaber A Y, Abdelaziz A A & Aida M S, *J King Saud Univ Sci*, 27 (2015) 356.
47 Ahmad R, Mahmoudi T, Ahn M S & Hahn Y B, *Biosens Bioelectron*, 100 (2018) 312.
48 Ahmad R & Hahn Y B, *J Colloid Interface Sci*, 512 (2018) 21.
49 Ahmad R, Ahn M S & Hahn Y B, *J Colloid Interface Sci*, 498 (2017) 292.
50 Schmidt-Mende L & MacManus-Driscoll J L, *Mater Today*, 10 (2007) 48.
51 Hosseinmardi A, Shojaee N, Keyanpour-Rad M & Ebadzadeh T, *Ceram Int*, 38 (2012) 1975.
52 Balegar S U, Srinatha N, Shashidhar R & Raghu A, *Mater Today Proc,* 92 (2023) 1453.
53 Hassan A T, Hassan E S & Abdulmunem O M, *J Mech Behav Mater*, 30 (2022) 304.
54 Carol-Coronel F J, Tobia D, Lima E, Sánchez R D & Saleta M E, *Mater Res Bullet*, 159 (2023) 112104.
55 Flak D, Braun A, Mun B S, Döbeli M, Graule T & Rekas M, *Proc Eng*, 47 (2012) 257.
56 Belamri Z, Darenfad W & Guermat N, (2023). *J Nono-Electron Phys*, 15(2023) 02026.
57 Zhang Y, Du G, Yang X, Zhao B, Ma Y, Yang T & Yang S, *Semicond Sci Technol*, 19 (2004) 755.
58 Khun K, Ibupoto Z H, AlSalhi M S, Atif M, Ansari A A & Willander M, *Materials*, 6 (2013) 4361.
59 Li C P, Yang B H, Wang X C, Wang F, Li M J, Su L & Li X W, *Appl Surf Sci*, 257 (2011) 5998.
60 Hammouda A, Canizarès A, Simon P, Boughalout A & Kechouane M, *Vib Spectrosc*, 62 (2012) 217.
61 Calizo I, Alim K A, Fonoberov V A, Krishnakumar S, Shamsa M, Balandin A A & Kurtz R, *Proc SPIE,* 6481 (2007) 64810.
62 Alim K, Fonoberov V A, Shamsa M & Balandin A A, *J Appl Phys*, 97 (2005) 124313.

63 Ashkenov N, Mbenkum B N, Bundesmann C, Riede V, Lorenz M, Spemann D & Monemar B, *J Appl Phys*, 93 (2003) 126.
64 Kara K, Tüzemen E Ş & Esen R, *Turk J Phys*, 38 (2014) 238.
65 Radjehi L, Aissani L, Djelloul A, Saoudi A, Lamri S, Nomenyo K & Sanchette F, *Metall Mater Eng*, 29 (2023) 37.
66 Aboud A A, Al-Dossari M, AbdEL-Gawaad N S & Magdi A, *Phys Scr*, 98 (2023) 095958.
67 Thongam D D, Gupta J & Sahu N K, *SN Appl Sci*, 7 (2019) 1030.
68 Jayarambabu N, Kumari B S, Rao K V & Prabhu Y T, *Int J Multidiscip Adv Res Trends*, 2 (2015) 273.
69 Kayani Z N, Iqbal M, Riaz S, Zia R & Naseem S, *Mater Sci - Pol*, 33 (2014) 515.
70 Amudhavalli B, Mariappan R & Prasath M, *J Electron Mater,* 53 (2023) 535.
71 Liu Y, Zhang H, Zhang Z, Xie Y & Xie E, *Appl Surf Sci*, 257 (2010) 1236.
72 Wisitsoraat A, Tuantranont A, Comini E, Sberveglieri G & Wlodarski W, *Thin Solid Films*, 517 (2009) 2775.
73 Nag P & Sujatha D P, *Trans Indian Ceram Soc*, 74 (2015) 129.
74 Yao M, Ding F, Cao Y, Hu P, Fan J, Lu C, Yuon F & Shi C*, Sens Actuators B: Chem*, 201 (2014) 265.
75 Zheng L, Zheng Y, Chen C, Zhan Y, Lin X, Zheng Q, Wei K & Zhu, J, *Inorg Chem*, 48 (2009) 1819.
76 Wang L, Kang Y, Liu X, Zhang S, Huang W & Wang S, *Sens Actuators B: Chem*, 162 (2012) 237.
77 Sarkar A, Maity S, Chakraborty P & Chakraborty S K, *J Electron Mater*, 46 (2017) 5485.